

空心圆柱体 GCr15 钢淬火过程的计算机模拟

姚新, 顾剑锋, 胡明娟, 张伟民

(上海交通大学高温材料及高温测试开放实验室, 上海 200030)

摘要: 用有限元法研究了 GCr15 钢圆柱体在油淬过程中的温度、组织及应力变化。在实测了淬火油换热系数的基础上, 对轴对称空心圆柱体淬火时的温度场和组织场进行了模拟。同时运用热弹塑性理论, 对圆柱体内外表面点及中心点应力的演化过程进行了模拟。模拟结果表明: 圆柱体内表面的冷速小于外表面。在淬火初期, 由于热应力的作用使工件表面受拉而心部受压, 在发生应力反向前, 发生了组织转变, 并使表面应力迅速转向, 在应力达到最低点后又逐渐回升, 最后表面形成了拉应力。心部的应力变化正好相反, 最终形成了组织应力型的内应力分布。

关键词: 淬火; 计算机模拟; 内应力; 轴承钢

中图分类号: TB115; TG156 **文献标识码:** A **文章编号:** 1009-6264(2003)01-0078-04



温度-组织-应力/应变模拟是淬火过程计算机模拟的主要内容^[1]。一般来讲, 淬火过程的模拟起始于均一的淬火温度, 而且初始内应力设为零。由于淬火过程涉及复杂的非线性问题, 人们通常用有限元法来模拟淬火过程中的各种变化。圆柱体是最常见的形状之一, 而且可以采用相对简单的轴对称问题来处理, 因此成为淬火过程模拟中最常见的形状。Denis^[2], Gü^[3], Wang^[4] 等人对不同材料圆柱形工件的淬火过程从不同的角度进行了模拟, 而且得出了与实验结果相符的结论。

本文采用通用有限元软件 MSC. Marc 结合用户自定义子程序对 GCr15 空心圆柱体淬火过程中内应力的分布及变化进行了研究。首先根据实测的淬火油的换热系数计算温度场, 而后根据温度场计算组织及其应力的分布。计算中同时考虑了相变潜热及其随温度变化的材料性能。

1 计算模型

热传导的计算中考虑了变物性、相变条件、相组成变化及非线性边界条件, 其控制方程为^[5]:

$$\left[\frac{\partial^2 T}{\partial r^2} + \frac{1}{r} \frac{\partial T}{\partial r} + \frac{\partial^2 T}{\partial z^2} \right] + \dot{q} = c \frac{\partial T}{\partial t} \quad (1)$$

相应的边界条件及初始条件分别为:

$$- \left[\frac{\partial T}{\partial r} n_r + \frac{\partial T}{\partial z} n_z \right] = h(T_s - T_m),$$
$$T(r, z, t) |_{t=0} = T_{\text{initial}} \quad (2)$$

式中, h 为表面换热系数, T_s 和 T_m 为工件表面温度及介质温度, λ 、 ρ 、 c 分别为材料的导热系数、密度和比热容, 它们是相组成及温度的函数。

由于本文用到的试样尺寸较小, 油淬后得到马氏体及少量的残留奥氏体, 因此在模拟计算中仅考虑了马氏体相变。根据 Magee 公式, 马氏体形成的体积分数为^[6]:

$$M = 1 - \exp[-0.011(M_s - T)] \quad (3)$$

淬火过程中总应变增量可分为以下几个部分:

$$d_{ij} = d_{ij}^e + d_{ij}^p + d_{ij}^v \quad (4)$$

其中 d_{ij}^e 、 d_{ij}^p 分别为弹性应变增量和塑性应变增量; d_{ij}^v 是由体积变化所造成的应变增量, 包括热应变增量 d_{ij}^{th} 和组织应变增量 d_{ij}^{tr} 。

所用空心圆柱体的外径 $R = 15\text{mm}$, 内径 $r = 7.5\text{mm}$, 长度 $l = 60\text{mm}$ 。其几何形状可视为两维轴对称问题。取工件轴截面的 1/2 进行模拟, 其有限元网格划分如图 1 所示。为提高求解精度, 对接近工件表面的部分进行了网络细分。工件内部的初始温度均一, 为 860°C , 淬至 20°C 的油中。在热分析过程中, 假定圆柱体的内外表面及其端面具有相同的表面换热系数, 且 AC 边的热流密度为零。在应力分析中, 设材料淬火前的初始应力为零, AC 边上节点沿轴线方向的位移为零。GCr15 的材料性能大多取自文献^[7], 列于表 1 中。奥氏体的热膨胀系数是通过图 2 所示

收稿日期: 2002-07-03; 修订日期: 2002-09-27

作者简介: 姚新(1973—), 男, 上海交通大学博士研究生。主要从事材料热加工过程的计算机模拟研究。E-mail: xin.yao@yahoo.com.

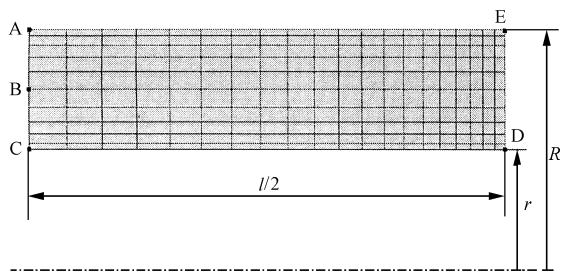


图 1 空心圆柱体中截面一半的网格划分

Fig.1 Finite element mesh of the tube in half of the cross section

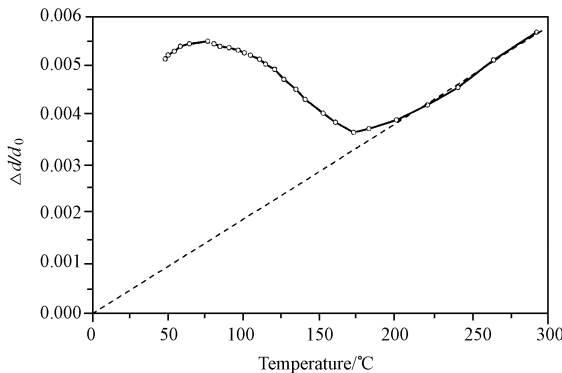


图 2 GCr15 钢的在无外加应力时的膨胀曲线

Fig.2 Expansion curve of GCr15 steel under no external stress

的膨胀曲线测出的。

2 换热系数的测量

实测了油的表面换热系数。实验采用方形探头，为消除相变的影响，选用 1Cr18Ni9Ti 不锈钢作为探头材料。在方形探头距表面不同距离处插入热电偶，加

热至 900 ℃均温后油冷。热电偶输出的电压信号经数据采集板滤波放大后进入 A/D 板进行模数转换。数据采集选用软件触发，采集速率为 0.01s。用反传热法对输出的数据进行处理，根据探头的几何形状，可用一维的有限差分来计算油的换热系数。图 3 为换热系数的计算结果，它随工件表面温度的变化而发生剧烈变化。

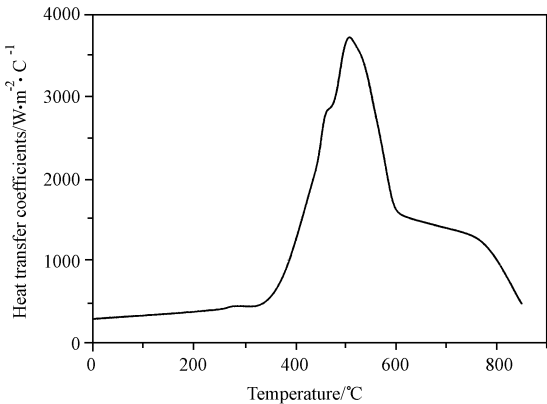


图 3 淬火油的表面换热系数

Fig.3 Heat transfer coefficients of quenching oil

3 计算结果与分析

图 1 中表面节点 A、C 及心部节点 B 的冷却曲线如图 4a 所示，由于工件壁厚较薄，冷却过程中表心温差并不大。内外表面虽然具有相同的换热系数，且初始温度相同，但它们的冷却速度却不同。外表面的冷速要高于内表面的冷速，因为外表面具有较大的表面积与淬火介质接触。

表 1 GCr15 钢的力学性能及热性能数据

Table 1 Mechanical and thermal properties of GCr15 steel

Temperatures and corresponding properties	Phases	20	100	300	600	900
Specific heat capacity, $C_p/(\text{W s kg}^{-1} \text{ } ^\circ\text{C}^{-1})$	A, M	553	-	787	-	729
Thermal conductivity, $\lambda/(\text{Wm}^{-1} \text{ } ^\circ\text{C}^{-1})$	A	15.0	-	18.0	21.7	25.1
	M	40.1	38.8	36.7	30.1	-
Density, $\rho/(\text{kg m}^{-3})$	A, M	7810	7810	7810	7810	7810
Thermal expansion coefficient, $\alpha/10^{-6} \text{ } ^\circ\text{C}^{-1}$	A	19.5	19.5	19.5	19.5	19.5
	M	10.5	10.5	10.5	10.5	-
Modulus of elasticity, E/GPa	A	200	190	185	165	120
	M	212	206	193	168	-
Poisson's ratio, ν	A, M	0.3	0.3	0.3	0.3	0.3
Modulus of plasticity, H/GPa	A, M	3.63	3.4	3.13	2.8	2.2
Initial yield strength, σ_0/MPa	A, M	343	-	230	140	52.5

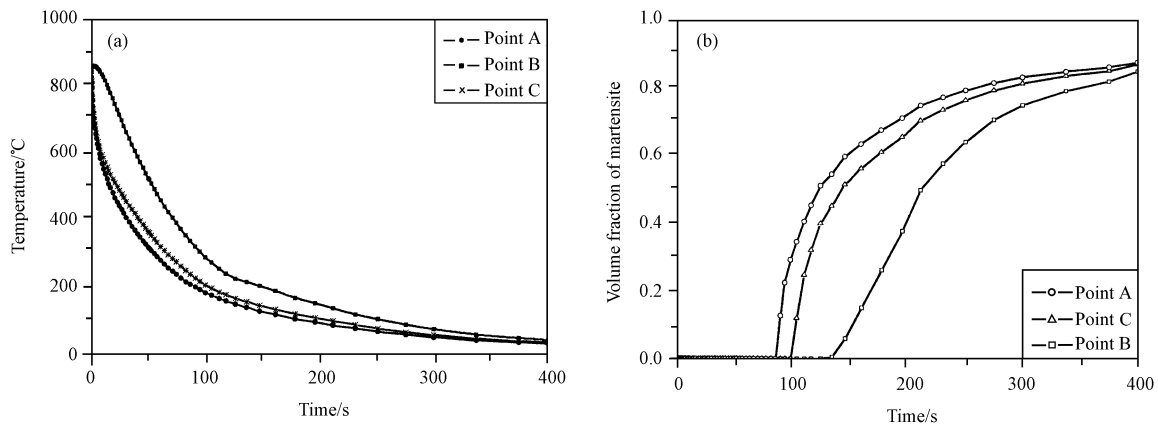


图 4 a) 油淬过程中表面及中心点的冷却曲线, 及 b) 马氏体转变量与油淬时间的关系 (A、B、C 点在图 1 中指明)

Fig. 4 a) Cooling curves of surface and center points during oil quenching, and b) martensite volume fraction versus quenching time

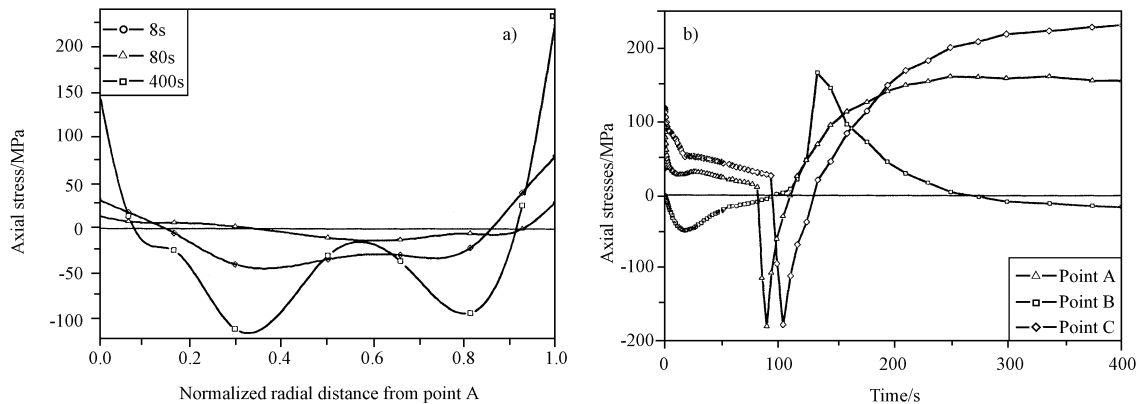


图 5 a) 油淬不同时间后工件内轴向应力的分布及, b) 内外表面点及中心点轴向应力随时间的变化 (A、B、C 点在图 1 中指明)

Fig. 5 a) Axial stresses distribution of the tube after oil quenching, and b) axial stress variation of the surface and center points with quenching time

淬火过程中的马氏体量与淬火时间的关系示于图 4b 中。在油淬 90s 后, 外表面首先析出马氏体, 400s 后, 表面和心部已有近 90% 的奥氏体转化为马氏体。

热应力和组织应力的共同作用使工件的内应力分布变得复杂, 因为两者往往起着相反的作用。在淬火初期, 由于表面的冷却速度比心部快, 表面收缩处于拉伸状态, 而心部处于压缩状态, 如图 5a 所示。表面温度的迅速下降造成了近表面处陡峭的温度梯度, 使表面点的轴向应力迅速上升至约 100MPa, 且内表面所受的拉应力大于外表面, 如图 5b 所示。随着表面温度的降低, 温度梯度也随之下落, 表面所受的轴向拉应力也不断减小。心部的应力状态则正好相反, 但变化较表面缓慢。在到达 50MPa 左右时, 所受的压应力也开始减小。若不发生相变, 表面和心部的应

力将缓慢地发生应力反向, 使表面受压而心部受拉^[8]。

但在发生应力反向前, 在油淬约 80s 时圆柱体外表面首先到达 M_s 点, 发生马氏体转变 (见图 4b)。由于马氏体转变的相变膨胀系数 (0.9849%) 大大高于其热膨胀系数 (奥氏体的热膨胀系数为 $1.9093 \times 10^{-5}/^\circ\text{C}$, 马氏体的热膨胀系数为 $1.0564 \times 10^{-5}/^\circ\text{C}$), 相变所引起的膨胀使表面由拉应力状态迅速变为压应力状态。而此刻心部还未发生相变, 表面膨胀所产生的压应力很可能超过屈服极限而引起塑性变形。随着温度的降低, 转变区向心部推移。次表层的相变减小了表层的压应力, 并于 120s 左右再次使应力反向。心部因表面的膨胀, 所受的拉应力也迅速上升。至大约 150s, 由于自身的马氏体转变, 拉应力逐渐减小, 并在 270s 左右发生应力反向, 应力再次成为负

值。经 400s 水淬后工件内的应力分布如图 5a 所示, 表面受拉应力而心部和次表层受压应力, 形成了组织应力型分布。

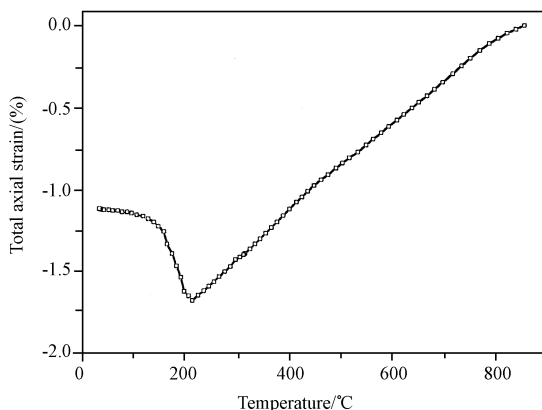


图 6 外表面点 A 在淬火过程中的总应变与温度的关系

Fig. 6 Variation of the total axial strain at surface point A versus temperature

图 6 为外表面点 A 在整个淬火过程中的总应变与温度的变化曲线,它是弹性应变、塑性应变、热应变及相变应变共同作用的结果。由图可见,在未发生相变前,热应变是主要应变形式。而当温度降至 230 以后,相变应变使曲线迅速上升,超过热应变而成为主要的应变形式。

4 结论

- 1) 应用热传导控制方程组求解 GCr15 空心圆柱体内外表面及中心点的温度变化及马氏体量的变化。
- 2) 实测淬火油的换热系数及 GCr15 轴承钢的热膨胀曲线,为模拟提供了必要的依据。
- 3) 应力模拟结果表明,热应力和组织应力的共同作用使工件内的内应力变化变得更为复杂。内外表面和心部应力在淬火过程中多次发生反向,最终获得组织应力型的应力分布。

参 考 文 献

- 1 Pan J, Li Y, Li D. The application of computer simulation in heat-treatment process of a large-scale bearing roller[J]. Journal of Material Processing Technology, 2002, 122:241 ~ 248.
- 2 Denis S, Gautier E, Simon A, Beck G. Stress-phase-transformation interaction-basic principles, modeling, and calculation of internal stresses[J]. Material Science and Technology, 1985, 1:805 ~ 814.
- 3 Gü C H, Tekkaya A E. Numerical investigation of non-homogeneous plastic deformation in quenching process[J]. Material Science and Engineering A, 2001, 319 ~ 312:164 ~ 169.
- 4 Wang K F, Chandrasekar S, Yang H T. Experimental and computational study of the quenching of carbon steel[J]. Journal of Manufacturing Science and Engineering, 1997, 119:257 ~ 265.
- 5 Cheng H, Huang X, Wang H. Calculation of the residual stress of a 45 steel cylinder with a non-linear surface heat-transfer coefficient including phase transformation during quenching[J]. Journal of Materials Processing Technology, 1999, 89 ~ 90:339 ~ 343.
- 6 徐祖耀. 马氏体相变与马氏体[M]. 北京: 科学出版社, 1981, 332.
- 7 钟顺思, 王昌生. 轴承钢[M]. 北京: 冶金工业出版社, 2000, 119.
- 8 Sen S, Aksakal B, Ozel A. Transient and residual thermal stresses in quenched cylindrical bodies[J]. International Journal of Mechanical Sciences, 2000, 42:2013 ~ 2029.

excellent adhesion after thermal cycling 100 times between 203 K and 423 K and there are no signs of delamination. Further, XRD confirms that the Ti layer reacts with the diamond substrates to form TiC and TiO species on the interface during post-deposition annealing 673 K \times 2 h in vacuum. The interface diffusion or reaction of Ti/diamond depend on not only the temperature but also the surface conditions of the diamond.

Key words: diamond; metallization; pre-firing; adhesion; thermal management

Effect of Conductivity of Solution on the Growth Rate and Compact of Micro-arc Oxidation Coating of LY12 Aluminum

LI Jun-ming, JIANG Bai-ling, JING Xiao-tian, WEN Xiao-bin (College of Material, Xi'an University of Technology, Xi'an shaanxi 710048, China)

Trans Mater Heat Treat, 2003, 24(1): 63 ~ 65, fig 4, table 0, ref 9.

Abstract: Effect of conductivity of solution on growing rate of micro arc oxidation ceramic coatings is studied. The relationship between the conductivity of solution and the insulating intensity that reflects the compact of the coatings is measured in terms of experiment. The results show that there is a approximately linear relationship between the growing rate and the conductivity of solution, and the insulating intensity of coatings, i. e., density of the coating, is increase at beginning and then decrease as the increase of conductivity of solution.

Key words: micro-arc oxidation; conductivity of solution; growth rate

Deposition of Nickel Films by Metal-Organic Chemical Vapor Deposition and Study on the Relevant Factors

PENG Dong-sheng, ZHAO Li-feng, LIU Shi-liang, XIE Chang-sheng (Faculty of Materials Science and Engineering, Huazhong University of Science and Technology, Hubei Wuhan 430074, China)

Trans Mater Heat Treat, 2003, 24(1): 66 ~ 69, fig 8, table 2, ref 10.

Abstract: Films of nickel are deposited by MOCVD technique from precursor Ni(CO)₄. The factors that influenced the deposition rate of nickel films, such as deposition temperature and pressure, are discussed in the paper. The microstructure and morphologies of the films are examined by means of X-ray diffraction (XRD), differential scanning calorimeter (DSC), scanning electron microscope (SEM). The microstructure and morphologies of the films changed with the experimental parameters, such as deposition temperature and deposition substrates. As a result, the better microstructured film and the rapid deposition rate are attained when the deposition temperature is about 150 °C. The visible crystals is found on copper substrate, otherwise, the part amorphous film can be obtained on glass substrate. The deposition rate is dropped as pressure in the reaction chamber is increased.

Key words: metal-organic chemical vapor deposition (MOCVD); nickel carbonyl; film

Effect of Ti Content on H₂ Escape Characteristic and Microstructure of Electrode Deposit Metal

WANG Xiao-dong¹, WEN Jiu-ba¹, WEI Jiu-shan², ZHANG Jing-hai² (1. Henan University of Science and Technology, Luoyang 471003, China; 2. Luoyang Ship Materials Institute, Luoyang 471003, China)

Trans Mater Heat Treat, 2003, 24(1): 70 ~ 72, fig 3, table 1, ref 6.

Abstract: Using alcohol hydrogen test, three point bending test, microstructure observation and fracture analysis, the effect of Ti content on diffusion hydrogen H₂ escape characteristic, microstructure and fracture morphology of electrode deposit metal were investigated. The results show that the diffusible hydrogen content and its escape velocity of the deposited metal decreased with increasing Ti content, acicular ferrite quantity and percentage of fibrous fracture also increased as well.

Key words: microstructure; diffusible hydrogen; escape characteristic; fracture morphology; percentage of fibrous fracture

Effect of External Electric Field on Microstructure And Diffusion Behavior of Friction Welding Joint of Dissimilar Materials During Post Weld Annealing Treatment

FU Li, DU Shui-geng, JIE Wan-qi (Department of Materials Science and Engineering, Northwestern Polytechnical University, Xi'an 710072, China)

Trans Mater Heat Treat, 2003, 24(1): 73 ~ 77, fig 4, table 1, ref 11.

Abstract: The friction welding joint of T2 copper and 1Cr18Ni9Ti stainless steel was employed to study the effect of post weld annealing treatment in the presence of electric field on the microstructure and diffusion behavior of the joint by electronic probe and optical microscope. The results show that electric field promotes the recrystallization of the weld metal, enhances the growth of recrystallization grains and increases the number of annealing twin. In addition, the diffusion zone of Fe and Cu widens in the presence of electric field. Moreover, the wider diffusion zone of the friction welding joint after annealing treatment with the increase of electric field intensity is found, and the electric field has greater influence on the diffusion distance when the specimen is connected to the cathode of the power supply.

Key words: annealing treatment with electric field; dissimilar material; friction welded joint

Numerical Simulation of the Quenching Process of GCr15 Steel Tube

YAO Xin, GU Jiannfeng, HU Ming-juan, ZHANG Wei-min (Public

Laboratory for High Temperature Material and High Temperature Test , Institute of Intelligent Technique for Heat Treat and Surface Engineering , Shanghai Jiaotong University , Shanghai 200030 , China) Trans Mater Heat Treat , 2003 ,24(1) : 78 ~ 81 ,fig 6 ,table 1 ,ref 8.

Abstract: A coupled thermal , structural and mechanical model was established to study the oil quenching process of GCr15 tube using Finite Element Method. After determining the heat transfer coefficient of oil , the temperature , microstructure and stress variations during quenching were analyzed. The results show that the cooling rate of the inner surface is slower than that of the outer surface. In the initial stage of quenching , the surfaces are in tensile and the core is in compressive because of the thermal stress. Under the effect of structural stress due to phase transformation , the axial stress in the surface is reversed to negative rapidly , and after reaching the nadir , gradually bounded back to positive. The stress variation in the center is just opposite , and a structural type internal stress state is formed after quenching.

Key words: quenching ; computer simulation ; internal stress ; bearing steel

Local Corrosion Failure Mode Recognition Based on Hopfield Neural Network

SONG Guang-xiong , HE Sheng-feng , CAO Hui , ZHANG Zheng , ZHONG Qun-peng (School of Material Science and Engineering , Beijing University of Aeronautics and Astronautics , Beijing 100083 , China)

Trans Mater Heat Treat , 2003 ,24(1) : 82 ~ 84 ,89 ,fig 5 ,table 1 ,ref 8.

Abstract: To develop the reasoning and learning model for identification of corrosion failure mode , the prototype of Hopfield neural network was utilized. The identification capacity of Hopfield

neural network is limited by the number of neural cells in the network. A grading method was introduced to overcome the above limitation. With the procedure of corrosion failure analysis and the utilization of object oriented programming (OOP) object oriented programming and database technology , an intelligent expert system for corrosion failure identification was developed and presented , which is capable of learning from knowledge inputted.

Key words: neural network ; corrosion failure ; failure analysis ; expert system

Numerical Simulation Research of Crater Formation Induced by High Current Pulsed Electron Beam Bombardment

QIN Ying , WU Ai-min , ZOU Jian-xin , LIU Yue , WANG Xiao-gang , DONG Chuang (State Key Laboratory for Materials Modification by Laser , Ion and Electron Beam , Dalian University of Technology , Dalian 116024 , China)

Trans Mater Heat Treat , 2003 ,24(1) : 85 ~ 89 ,fig 5 ,table 1 ,ref 15.

Abstract : Numerical simulation is used to describe the rapid heating , cooling , melting and solidification processes in aluminum bombarded by high current pulsed electron beam. When pulse duration is 0.5μs and the absorbed energy density is 3J/cm² , the calculated temperature field indicates that the melted layer depth is about 2.5μm , which is in agreement with TEM observation , and the melting occurs from 0.4μs to 1.6μs. The rate of heating and cooling is up to 10⁸ ~ 10⁹ K/s. The melting and resolidification start at depths of 1.4μm and 2.5μm , respectively. The force of volume expansion is about 275MPa , and the eruptible rate of melting matter is about 1330m/s. Such a sublayer melting is responsible for the formation of craters on the surface , confirming the experimental results.

Key words: high current pulsed electron beams (HCPEB) ; numerical simulation ; crater